ORGANOMETALLICS

Article

pubs.acs.org/Organometallics

Impact of a Picolinate Ancillary Ligand on Phosphorescence and Fluoride Sensing Properties of $BMes_2$-Functionalized Platinum(II) Compounds

Soo-Byung Ko,[†] Jia-Sheng Lu,[†] Youngjin Kang,[‡] and Suning Wang*[,†]

[†]Department of Chemistry, Queen's University, Kingston, Ontario, K7M 3N6, Canada

[‡]Division of Science Education, Kangwon National University, Chuncheon 200-701, Republic of Korea

Supporting Information

ABSTRACT: Two new dimesitylboron ($BMes_2$)-functionalized 2-phenylpyridine cyclometalated Pt(II) complexes (**2** and **3**) with a picolinate or a methyl-picolinate as the ancillary ligand have been synthesized via a one-pot procedure at ambient conditions with high yields (>70%). The crystal structures of these Pt(II) complexes were determined by single-crystal X-ray diffraction analysis, which revealed the presence of extended π-stacking interactions in the crystal lattice of **2** and discrete dimer formation in the lattice of **3**. Both complexes exhibit dual phosphorescence emission in solution at room temperature under N_2 atmosphere. These unusual photophysical properties have been systematically investigated by spectroscopic and computational studies, which established that the phosphorescent dual emission originates from admixture of ^{3}LLCT and ^{3}ILCT/^{3}MLCT transitions. Fluoride titration experiments were conducted to further confirm the origin of phosphorescence in these compounds. The phosphorescent properties and the phosphorescent response toward fluoride ions by compounds **2** and **3** are distinctly different from the previously known $BMes_2$-functionalized N^C-chelate Pt(II) compounds, which are attributed to the introduction of the low-lying π^* orbital by the picolinate ancillary ligand in the Pt(II) compounds.

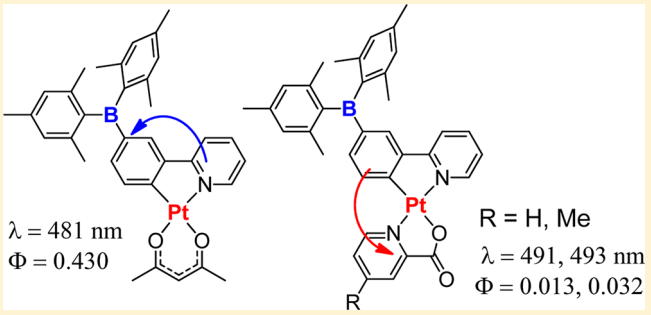

INTRODUCTION

Triarylboron compounds with sterically bulky aryl groups such as mesityl have recently attracted much research interest because of their broad applications in nonlinear optical materials,[1] charge transfer materials and emitters in organic light emitting devices (OLEDs),[2] and highly selective small anion sensors such as fluoride and cyanide.[3] When triarylboron groups are connected by proper electron-donating groups through π conjugation, bright luminescent compounds can be achieved.[2,4] Such compounds have been often applied as switch-off sensors for fluoride anions because the binding of a fluoride to the boron center quenches the charge transfer (CT)-based luminescence. Furthermore, we have shown that the binding of fluoride anions to a triarylboron center in spatially separated donor−acceptor molecules can suppress charge transfer and activate alternative emission pathways such as $\pi-\pi^*$ transitions, leading to switch-on sensors for fluoride ions.[5] The attachment of a triarylboron moiety to a transition metal center has been shown to greatly enhance metal-to-ligand charge transfer (MLCT)[6] and phosphorescence efficiency.[6] This has led to the development of phosphorescence-based sensing systems for anions using triarylborane-functionalized transition metal complexes such as Hg(II),[7] Ir(III),[8] Re(I),[9a,b] Ru(II),[9c,d] and Pt(II)[6b,c,10] and high efficiency OLEDs based on Pt(II) compounds.[6f−j]

We have recently reported the impact of the $BMes_2$ (Mes = mesityl) location on the phosphorescence of Pt(*Bppy*)(acac) compounds (ppy = 2-phenylpyridine).[11] We have found that the *meta*-$BMes_2$-functionalized ppy ligand *m-Bppy* can lead to about 60 nm phosphorescence blue shift of its Pt(II) compound, (*m-Bppy*)Pt(acac) (**1**, Chart 1), relative to the *para*-substituted compound Pt(*p-Bppy*)(acac). This provides an effective way to tune the emission color of N^C-chelate Pt(II) compounds. Among phosphorescent compounds, blue phosphorescent molecules are most in demand because stable blue phosphorescent compounds in OLED devices remain challenging and rare. Although compound **1** has bright phosphorescence and impressive performance in OLEDs,[11] it is a blue-green emitter with λ_{em} = 481 nm. To examine whether changing the acetylacetonato ancillary ligand to a picolinate ligand can shift the emission color of the Pt(II) compound further toward blue and to develop new dual-emissive Pt(II) compounds, we have designed and synthesized new (*m-Bppy*)Pt(picolinate) complexes. The choice of the picolinate

Received: November 19, 2012

   dx.doi.org/10.1021/om301112u | *Organometallics* XXXX, XXX, XXX−XXX

Chart 1

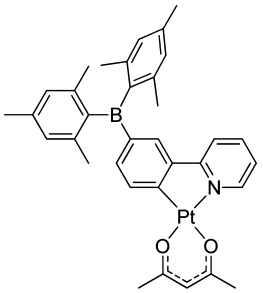

*(m-Bppy)*Pt(acac) (**1**)

ligand as the ancillary ligand is based on the fact that several nonborylated N^C-chelate Pt(II) compounds with the picolinate ancillary ligand have been demonstrated for applications in OLEDs.[12] In addition, it is well known that the picolinate ligand has a higher ligand field strength than that of acetylacetonate (acac) and its derivatives,[13] thus may be very useful in achieving highly efficient blue or blue-green phosphorescent Pt(II) compounds by stabilizing the occupied d orbitals and increasing d−π^* transition energy. In fact, highly efficient Ir(III) phosphorescent compounds using picolinate ligands are well known in the literature, with an emissive triplet state that is much higher in energy than that of acac derivatives.[13,14] We have found that the picolinate ancillary ligand has a dramatic impact on phosphorescence and fluoride sensing properties of the *m-Bppy*-chelate Pt(II) compounds. The details of these results for our investigation and discussion are reported herein.

RESULTS AND DISCUSSION

Syntheses. The synthetic procedures and conditions for the new Pt(II) complexes (**2** and **3**) are shown in Scheme 1. The *m-Bppy* ligand was synthesized using a modified procedure reported by Park and co-workers.[8a] The traditional method for synthesizing cyclometalated Pt(II) picolinate complexes involves two steps by first heating 2.0 to 2.5 equiv of the cyclometalating ligand with K_2PtCl_4 in solution to produce a dichloro-bridged Pt(II) dimer, which is then heated over 100 °C with 2-picolinic acid in the presence of excess sodium carbonate to obtain the final product with moderate yields.[12] These harsh basic reaction conditions, however, are not suitable for the synthesis of organoboron-containing Pt(II) compounds due to the Mes_2B−C bond cleavage at high reaction temperature.[15] To overcome this problem, a one-pot synthetic method[16] for cyclometalated Pt(II) β-diketonate compounds developed recently by our group is modified and used in the synthesis of compounds **2** and **3**. The (*m-Bppy*)$PtMe(SMe_2)$ intermediate is generated by the reaction of *m-Bppy* and $[PtMe_2(SMe_2)]_2$ in THF at room temperature for 2 h. The addition of 1.5 equiv of picolinic acid leads to the formation of the corresponding (*m-Bppy*)Pt(II) picolinate products (**2** and **3**) as yellow solids under mild conditions, which are isolated by column chromatography on silica gel with high yields (70−72%). These two Pt(II) complexes are air stable in solution and the solid state. These complexes have been fully characterized by NMR spectroscopy, elemental analyses, and single-crystal X-ray diffraction analyses.

Crystal Structures. The crystal structures of **2** and **3** determined by X-ray diffraction are shown in Figure 1 and 2, respectively, along with important bond lengths and angles. One important feature revealed by the crystal structures is that the nitrogen donor atoms in both compounds have a *trans*-geometry. NMR spectra indicate that the *trans*-isomer is the only product for both **2** and **3**. This may be caused by the strong *trans*-directing effect of the phenyl group that favors the weaker carboxylate donor over the pyridyl donor. In addition, the preferential H bond formation between the carboxylate oxygen atom O(1) and the *ortho*-H atom of the pyridyl ring (N−H···O = 2.41 Å in **2** and 2.39 Å in **3**) may also play a role in the exclusive formation of the *trans*-isomer. Similar *trans*-geometry in related (*ppy*)Pt(N^O) compounds has been reported previously.[17] Despite the substitution by a methyl group in the picolinate ancillary ligand in compound **3**, the bond lengths and the chelating bond angles around the Pt(II) are similar in both compounds.

Scheme 1. Synthetic Procedure for the Pt Complexes 2 and 3

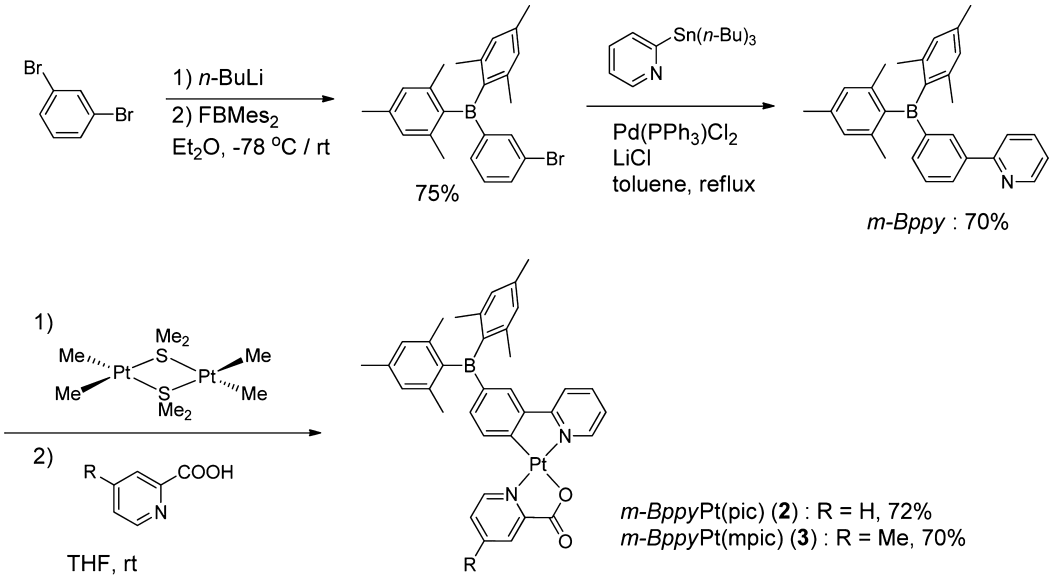

dx.doi.org/10.1021/om301112u | Organometallics XXXX, XXX, XXX−XXX

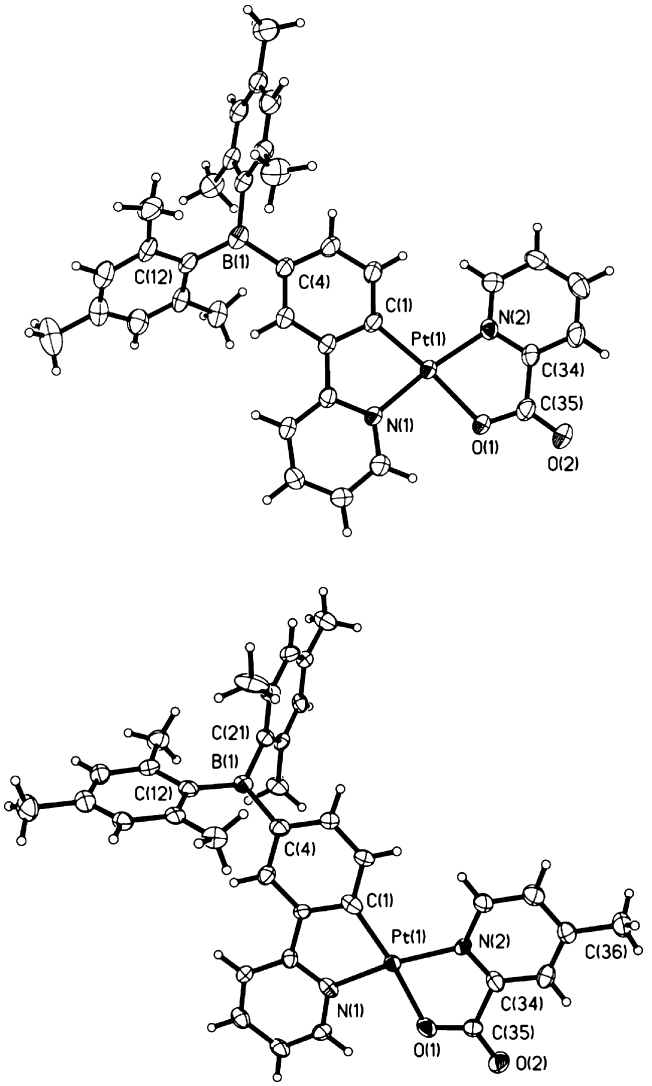

Figure 1. Structure diagrams of **2** (top) and **3** (bottom) with 50% thermal ellipsoids and labeling schemes for the key atoms. Important bond lengths (Å) and angles (deg) for **2**: Pt(1)−N(1) 2.000(4), Pt(1)−C(1) 2.000(4), Pt(1)−N(2) 2.038(4), Pt(1)−O(1) 2.093(3), B(1)−C(4) 1.562(7), B(1)−C(12) 1.581(7), B(1)−C(21) 1.576(7) Å, N(1)−Pt(1)−N(2) 173.23(14), C(1)−Pt(1)−O(1) 173.93(15), C(1)−Pt(1)−N(1) 80.72(16), N(2)−Pt(1)−O(1) 79.75(13)°; for **3**: Pt(1)−N(1) 1.977(8), Pt(1)−C(1) 2.011(12), Pt(1)−N(2) 2.024(9), Pt(1)−O(1) 2.094(9), B(1)−C(4) 1.555(17), B(1)−C(12) 1.570(16), B(1)−C(21) 1.591(15), N(1)−Pt(1)−N(2) 171.88(3), C(1)−Pt(1)−O(1) 173.5(3), C(1)−Pt(1)−N(1) 80.8(4), N(2)−Pt(1)−O(1) 79.1(3).

The key difference between compounds **2** and **3** is their distinct intermolecular interaction patterns in the crystal lattices. As shown in Figure 2, molecules of **2** form Pt(II) dimers with a Pt···Pt separation distance of 3.710 Å. The pyridyl ring of the ppy chelate and the pyridyl ring of the picolinate are directly on top of each other, with the π-stacking distances ranging from 3.53 to 3.80 Å. Most significantly, the Pt(II) dimers of **2** further stack through the pyridyl rings with π-stacking distances of 3.70−3.76 Å, which leads to the extended π-stacking in the crystal lattice. A Pt(II) dimer is also present in the crystal lattice of **3**, as shown in Figure 3. However, the Pt···Pt separation distance (4.125 Å) is much longer than that in **2**. In fact the Pt atom is much closer to the

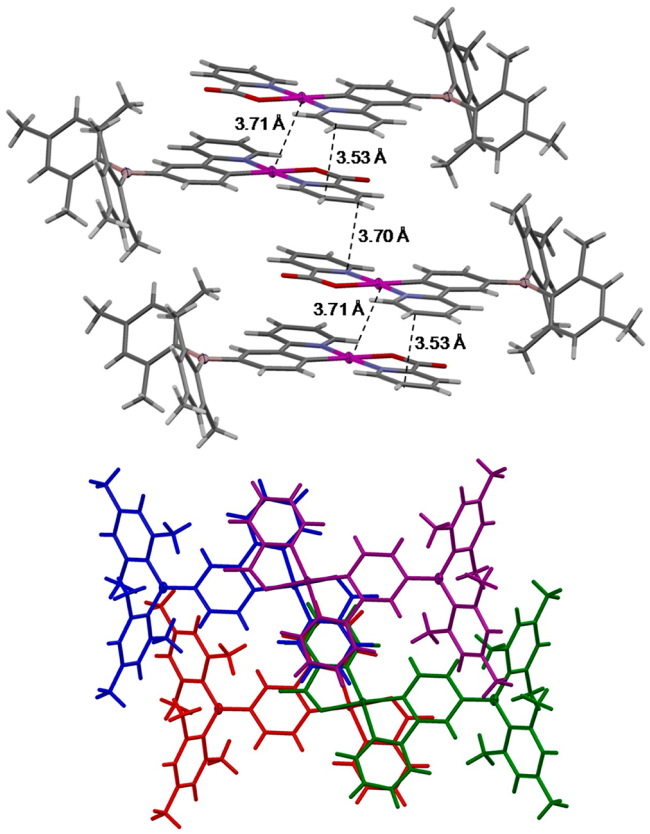

Figure 2. Diagrams showing intermolecular stacking of complex **2**, the Pt···Pt separation distance, and the shortest π-stacking distances. Top: Side view. Bottom: Top view of four color-coded molecules.

picolinate N atom from a neighboring molecule (3.76(1) Å) than to the other Pt atom (as indicated by the red dashed line in Figure 3). The π-stacking interaction within the dimer of **3** is much less than that observed in **2**, as shown by the top view of the stacking diagram of **3**, and resembles that of the acac analogue,[11] compound **1**. Most noteworthy is that no interdimer π-stacking is present in the crystal lattice of **3**. There are some hydrogen bond interactions between the pyridyl of the ppy ligand and the oxygen atom of the picolinate ligand between the dimers as shown in Figure 3. Overall, the crystal structural data indicate that intermolecular π-stacking interactions and Pt···Pt interactions in **3** are much weaker than those in **2**, which can be attributed to the methyl substituent in the picolinate ligand in **3**, which considerably reduces the π-stacking involving the picolinate pyridyl ring and the *ppy* pyridyl ring. Compared to the acac analogue, compound **1** (Pt···Pt distance = 4.64−4.67 Å),[11] the Pt···Pt separation distances of **2** and **3** are shorter, indicating that the picolinate ligand has a greater tendency to promote intermolecular π-stacking, which may be attributed to the aromatic pyridyl ring.

Absorption Spectra. The absorption spectra of the free ligand *m-Bppy* and their Pt(II) complexes **2** and **3** were recorded in CH_2Cl_2 solution and are shown in Figure 4 and Table 1. The π to π^* absorption band of *m-Bppy* at 313 nm is blue-shifted approximately by 16 nm compared to that of earlier reported *para*-substituted *p-Bppy*,[10b] which can be attributed to the greater stabilization of the ground state by *meta* substitution.[11] Compared to the free ligand *m-Bppy*, the π to π^* absorption bands of Pt(II) complexes **2** and **3** are red-shifted by ∼13 nm with increased absorbance, which can be

dx.doi.org/10.1021/om301112u | *Organometallics* XXXX, XXX, XXX−XXX

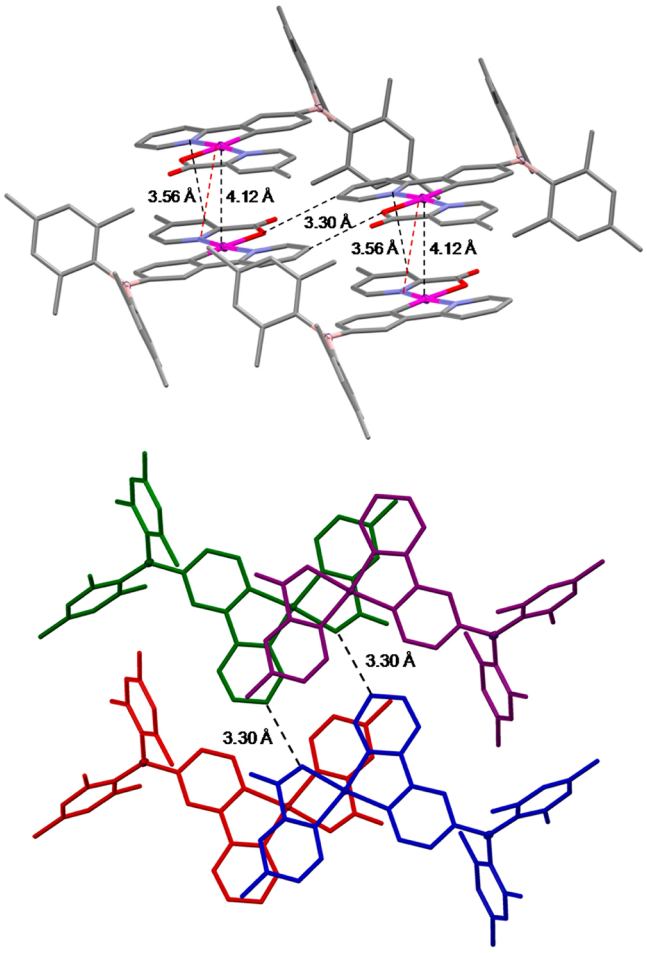

Figure 3. Diagrams showing intermolecular stacking of complex **3**, the Pt···Pt separation distance, H-bond distances, and the shortest π-stacking distances. Top: Side view. Bottom: Top view of four color-coded molecules.

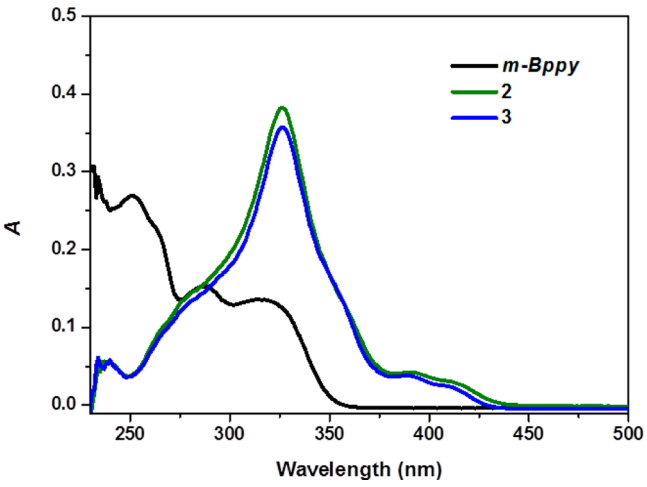

Figure 4. UV–vis absorption spectra of *m-Bppy* and its Pt(II) complexes **2** and **3** in CH_2Cl_2 (1.0×10^{-5} M).

explained by the π-conjugation enhancement by metal chelation. In addition, these Pt(II) complexes show two well-resolved absorption bands in the 380–450 nm region with moderate extinction coefficients. The absorption band at approximately 390 nm for **2** (4222 $M^{-1}cm^{-1}$) and **3** (3798

Table 1. Absorption and Luminescence Data

	absorption[a]	emission, 298 K[a]		emission, 77 K[c]
compound	λ_{max} (nm), ε (10^4 cm^{-1} M^{-1})	λ_{max} (nm)/τ_p (μs)	Φ_p[b]	λ_{max} (nm)/τ_p (μs)
m-Bppy	251 (2.70), 287 (1.53), 313 (1.36)	397	0.081	364
1[d]	271 (1.85), 327 (3.01), 344 (2.56)	481/8.7 (2)	0.430	478/9.4 (1)
2	261 (2.40), 326 (3.69), 390 (0.42), 415 (0.35)	450/14.1 (9), 493/8.0 (5)	0.013	442/29.6 (1), 482/16.2 (2)
3	263 (2.38), 326 (3.79), 388 (0.27), 412 (0.23)	450/18.8 (0), 491/8.2 (9)	0.032	440/34.6(5), 481/15.6 (8)

[a]The spectra were measured in degassed CH_2Cl_2 solution: [M] = 1.0×10^{-5}. [b]The quantum efficiency for the free ligand was measured under air using 9,10-diphenylanthracene as the standard (Φ = 0.95).[18] For the Pt(II) complexes, the quantum efficiency was obtained under N_2 atmosphere using *fac*-Ir(ppy)$_3$ as the standard (Φ = 0.97).[19] [c]Measured in 2-methyltetrahydrofuran solution. [d]From ref 11.

M^{-1} cm^{-1}) can be assigned to an intraligand charge transfer (ILCT)/MLCT mixed ligand-to-ligand charge transfer (LLCT) transition. The other lower lying absorption band at 415 nm (2700 M^{-1} cm^{-1}) for **2** and 412 nm (2300 M^{-1} cm^{-1}) for **3** can be assigned to mixed transitions involving LLCT mixed with ILCT/MLCT transitions. These assignments are also supported by Time-dependent density functional theory (TD-DFT) calculation results (see the TD-DFT section).

Luminescence Spectra. The luminescent spectra of the free ligand and their Pt(II) complexes **2** and **3** in CH_2Cl_2 at room temperature are shown in Figure 5 and Table 1. The free

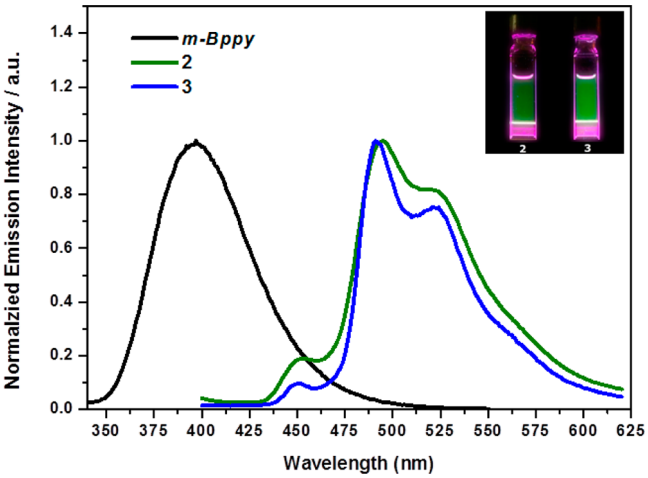

Figure 5. Luminescent spectra of *m-Bppy* and its Pt(II) complexes **2** and **3** in CH_2Cl_2 (1.0×10^{-5} M) under N_2 at 298 K.

m-Bppy ligand displays blue luminescence at 397 nm (Φ = 0.081), which is hypsochromic shifted by 12 nm compared to that of the *para*-substituted *Bppy*.[10c] The Pt(II) complexes **2** and **3** show green phosphorescence when excited in their lowest energy absorption bands. Both compounds show two distinct emission peaks at 450 nm and 491 or 493 nm, respectively, that are sensitive to oxygen. The relative intensity ratio of these two peaks is different for **2** and **3**. The emission lifetime of the peak at 450 nm (τ_p = 14.1–18.0 μs) is longer than that at 491 nm (or 493 nm) (τ_p = 8.0–8.2 μs). From the position and the structureless shape, the emission peak at 450

dx.doi.org/10.1021/om301112u | *Organometallics* XXXX, XXX, XXX–XXX

nm is assigned to the ILCT/MLCT mixed ^{3}LLCT transition.[20] The emission peak at 491−493 nm shows vibronic progressions of 1168 cm^{-1}, which become more apparent in the 77 K spectra recorded in 2-methyltetrahydrofuran frozen glass (Figure 6).

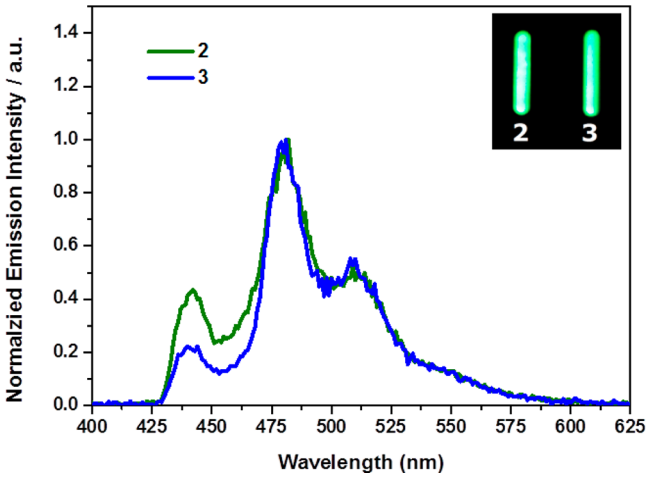

Figure 6. Time-resolved (delay time = 180 μs) phosphorescence spectra of **2** and **3** in 2-methyltetrahydrofuran at 77 K.

This emission peak is most likely from ^{3}ILCT and ^{3}LLCT transitions mixed with MLCT characters, as indicated by the TD-DFT calculation results. The emission spectra of both complexes display a small regiochromic blue shift with the peak at ∼490 nm being shifted to ∼480 nm and a substantial increase of the decay lifetime upon cooling to 77 K. Compared to the acac compound **1** and related substituted *m*-B*ppy* Pt(II) acac compounds, the phosphorescent quantum efficiencies of **2** and **3** are very low (Φ = 0.013 for **2** and 0.032 for **3**), which may be attributed to intermolecular interactions and the ^{3}LLCT contribution to the phosphorescence. In fact, compound **2** was found to display a strongly concentration dependent phosphorescence, as shown in Figure 7. At concentrations above 1.0 × 10^{-4} M, a broad emission band at ∼625 nm, characteristic of Pt(II) excimer emission,[21] was observed, accompanied with an emission color change from green to orange. This is in agreement with the extensive intermolecular

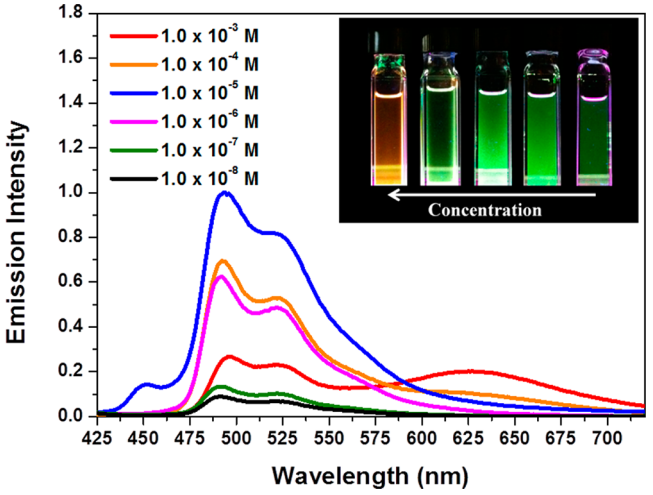

Figure 7. Concentration effects for the emission spectra of **2** in CH_2Cl_2 at ambient temperature.

stacking phenomenon of **2** revealed by the crystal data. No strong concentration dependence of **3** was observed.

Electrochemical Properties. The oxidation and reduction potentials of the Pt(II) compounds were recorded using cyclic voltammetry (CV) in *N*,*N*-dimethylformamide (DMF). Both **2** and **3** show a quasi-reversible reduction wave that is characteristic of the picolinate ligand and at much more positive potentials than that of compound **1**, which displays a reduction wave typical of $BMes_2$.[10,11] A quasi-reversible oxidation wave was also observed for both compounds. Using the oxidation and the reduction potentials, the HOMO and LUMO energy levels of complexes **2** and **3** were estimated and are shown in Table 2. Compared to compound **1**, the LUMO

Table 2. Electrochemical Data[a]

complex	$E_{1/2}^{ox}$ (V)	$E_{1/2}^{red}$ (V)	optical energy gap (eV)	HOMO (eV)[b]	LUMO (eV)[c]
1[d]		−2.34	2.92	−5.49	−2.46
2	0.62	−2.18	2.80	−5.42[b] (−5.45[e])	−2.62
3	0.58	−2.25	2.83	−5.38[b] (−5.37[e])	−2.55

[a]The CV was recorded in DMF solution containing 0.10 M (n-Bu)$_4$PF$_6$ as the electrolyte, relative to E^o(Fc/Fc$^+$) = 0.55 V. [b]Estimated from the oxidation potentials.[22] [c]Estimated from the reduction potentials.[22] [d]From ref 11. [e]Estimated from the optical energy gap and the LUMO energy.

level of both **2** and **3** is significantly lower, while the HOMO level is approximately the same. This could be attributed to the greater electron affinity of the picolinate ligand, compared to the acac ligand in compound **1**. As a consequence, the LUMO level is no longer dominated by the boron moiety in **2** and **3**, in contrast to that observed in compound **1** and other $BMes_2$-functionalized N^C-chelate Pt(II) compounds with acac or its derivatives as the ancillary ligand.[11]

DFT Computational Results. The surfaces and energies of the frontier orbitals for **2** and **3** in the ground state are depicted in Figure 8. Complete diagrams for both complexes are provided in the Supporting Information. For both **2** and **3**, the HOMO involves contributions mainly from the d orbital of the Pt(II) center (33−34%), the π orbitals of the phenyl ring of *m*-*Bppy*, and the carboxylate of the picolinate ligand. In contrast, the LUMO is localized on the pyridyl rings of *m*-*Bppy* and picolinate with no contributions from the boron center at all, in agreement with the electrochemical data. This is in sharp contrast to all previously reported N^C-chelate Pt(II) compounds based on $BMes_2$-functionalized *ppy* and related ligands, in which the LUMO is consistently dominated by the boron center.[6f,10,11] In **2** and **3**, the main contribution of the $BMes_2$ group is found in the LUMO+2. The general trend of the calculated HOMO and LUMO energies and the HOMO−LUMO gap for compounds **2** and **3**, relative to those of **1**, at the ground state is shown in Figure 9, which is in good agreement with the experimental data shown in Table 2.

To understand the photophysical properties of **2** and **3**, TD-DFT calculations were performed to evaluate the vertical excitation energies of each complex for the lowest six singlet and three triplet states. The important low-lying singlet and triplet states are shown in Table 3 (also see Supporting Information for details). The calculation results show that the S_1 state is mainly from the HOMO → LUMO transition (95%) for both compounds. The T_1 state is also dominated by the HOMO → LUMO transition (67−68%). Thus, the S_1 and T_1

dx.doi.org/10.1021/om301112u | *Organometallics* XXXX, XXX, XXX−XXX

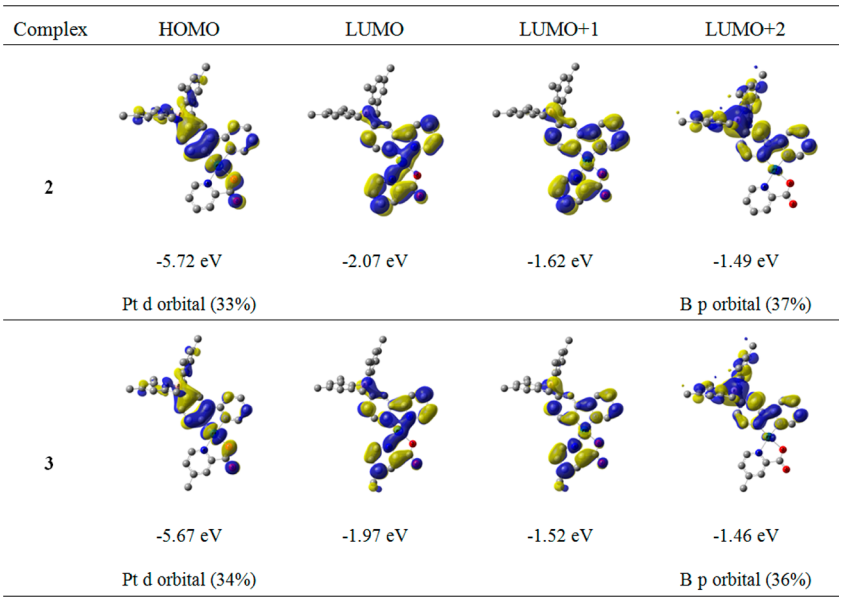

Figure 8. Isodensity surface plots and energies for frontier orbitals of **2** and **3** in the ground state (isodensity contour = 0.02 au).

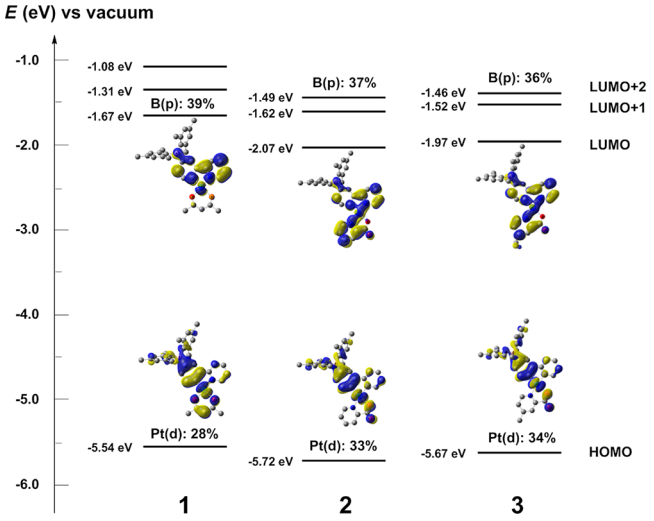

Figure 9. Calculated frontier orbital surface and energies for Pt(II) complexes **1**–**3**.

states can be assigned to LLCT mixed with ILCT/MLCT transitions. The phosphorescent emission peak at ~490 nm for both compounds can be attributed to the T_1 state. In comparison, the T_1 state of compound **1** involves mainly transitions localized on the *Bppy* ligand with a large contribution from the $BMes_2$ unit. Thus, the low phosphorescent quantum efficiencies of **2** and **3**, in comparison to that of **1**, may be attributed to the large contribution of the interligand or ligand-to-ligand CT transition to the T_1 state.

The S_2 state has the HOMO → LUMO+1 as the dominant transition for **2** and **3**. The T_2 state has mixed contributions from HOMO → LUMO and HOMO → LUMO+1 transitions and is 0.42 and 0.46 eV higher in energy than T_1, for **2** and **3**, respectively. The S_2 and T_2 can also be designated as ILCT/MLCT mixed LLCT transitions. The HOMO → LUMO+2 transition, which is mainly localized on the *m*-Bppy ligand with a large $BMes_2$ contribution, dominates the S_6 state (43% and 63% for **2** and **3**, respectively) and the T_3 state (46% and 57% for **2** and **3**, respectively). The intense absorption peak at 326 nm in **2** and **3** can be assigned to the S_6 state. Because the T_2 and T_3 states are close in energy (0.10–0.14 eV difference), the phosphorescence emission at 450 nm by **2** and **3** may have contributions from both states.

On the basis of the computational data, we suggest that the low phosphorescent quantum efficiencies of **2** and **3** are mainly

Table 3. TD-DFT Calculation Results for 2 and 3[a]

complex	state	transition energy	transition configuration	oscillator strength (*f*)
2	S_1	418.9 nm (2.96 eV)	HOMO → LUMO (95%)	0.0382
	S_2	366.0 nm (3.39 eV)	HOMO → LUMO+1 (86%)	0.0073
	S_6	342.2 nm (3.62 eV)	HOMO → LUMO+2 (43%)	0.2014
	T_1	478.0 nm (2.59 eV)	HOMO → LUMO (67%)	
			HOMO → LUMO+1 (12%)	
	T_2	412.2 nm (3.01 eV)	HOMO → LUMO (22%)	
			HOMO → LUMO+1 (31%)	
	T_3	391.7 nm (3.17 eV)	HOMO → LUMO+2 (46%)	
3	S_1	413.0 nm (3.00 eV)	HOMO → LUMO (95%)	0.0409
	S_2	360.3 nm (3.44 eV)	HOMO → LUMO+1 (77%)	0.0107
	S_6	341.5 nm (3.63 eV)	HOMO → LUMO+2 (63%)	0.2570
	T_1	475.9 nm (2.61 eV)	HOMO → LUMO (68%)	
			HOMO → LUMO+1 (9%)	
	T_2	404.1 nm (3.07 eV)	HOMO → LUMO (20%)	
			HOMO → LUMO+1 (21%)	
	T_3	391.1 nm (3.17 eV)	HOMO → LUMO+2 (57%)	

[a]TD-DFT was calculated at the B3LYP level using the LANL2DZ basis set for Pt and the 6-31G(d) basis set for all other atoms.

dx.doi.org/10.1021/om301112u | *Organometallics* XXXX, XXX, XXX–XXX

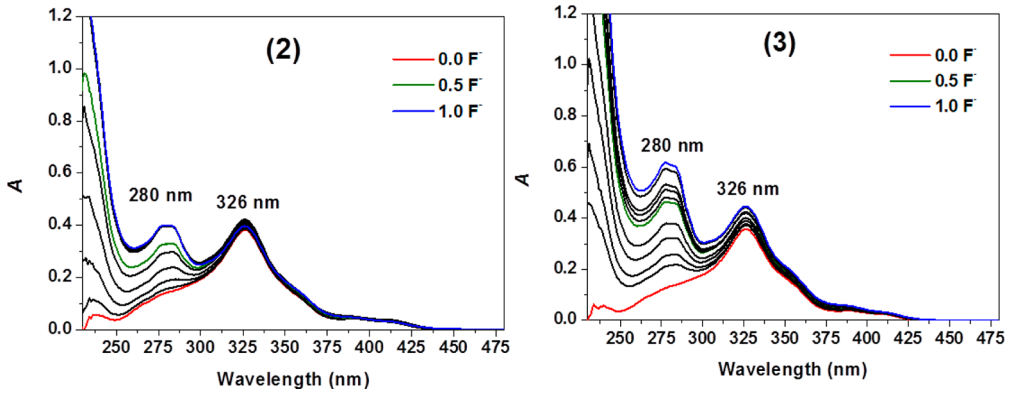

Figure 10. UV−vis spectral change of **2** and **3** (1.0×10^{-5} M) with the addition of $(n\text{-Bu})_4$NF in CH_2Cl_2.

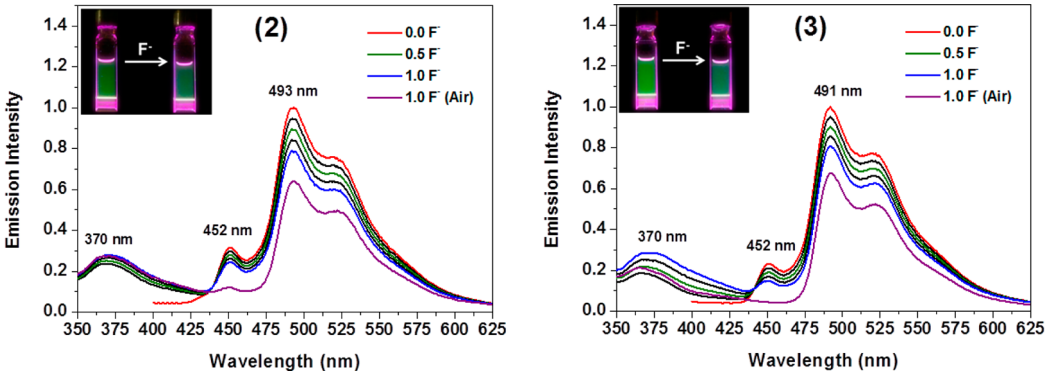

Figure 11. Phosphorescent spectral change of **2** and **3** (1.0×10^{-5} M) with the addition of $(n\text{-Bu})_4$NF in CH_2Cl_2 under a N_2 atmosphere.

caused by the T_1 state being dominated by charge transfer between *ppy* and the picolinate ligand (or ^{3}LLCT transitions). Thus, in order to achieve highly efficient phosphorescence in the $BMes_2$-functionalized N^C-chelate Pt(II) compounds, it is critical that the N^C-chelate chromophore centered transitions (^{3}LC or ^{3}ILCT) are the main contributions in the lowest triplet state with a significant involvement of the $BMes_2$ group.

Fluoride Titration. To further probe the origin of the phosphorescence displayed by **2** and **3**, we conducted fluoride titration experiments, which were monitored by UV−vis, emission, and ^{1}H and ^{19}F NMR spectra. The absorption spectral change of compounds **2** and **3** with the addition of *n*-NBu_4F is shown in Figure 10. The low-energy absorption bands for both compounds experience a slight red shift by ∼20−25 nm. The peak at 326 nm shows a significant intensity gain, while the high-energy band at 270−285 nm experiences a linear increase in intensity with the addition of F^-. TD-DFT computational data for the fluoride adducts $[NH_4][\mathbf{2F}]$ and $[NH_4][\mathbf{3F}]$ at the ground state indicate that the intense peak at ∼326 nm is from the S_{10} state with contributions mainly from a π (ppy)→π^* (ppy-picolinate) transition, which happens to be at a similar energy and with a similar oscillator strength to those of the S_6 state of **2** and **3**, thus explaining the small change of the low-energy absorption band with fluoride. All Pt(II) compounds were found to have a stronger binding with fluoride ions, compared to the free ligand, as evidenced by the binding constants of 1.00×10^7, 3.30×10^7, and 1.24×10^6 M^{-1}, for **2**, **3**, and the free *m-Bppy* ligand, respectively, obtained using the Benesi−Hildebrand analysis method.[23] This can be attributed to the chelation effect of the Pt(II) center, which is known to enhance the Lewis acidity of the boron center on the chelate backbone.[6b,c,10a,b] For more details, please refer to the Supporting Information.

As shown in Figure 11, the phosphorescence spectra of compounds **2** and **3** do not experience drastic emission energy change in the range 450−625 nm upon the addition of fluoride ions, in contrast to previously reported $BMes_2$-functionalized transition metal compounds that usually display a distinct emission energy and phosphorescent color change.[6−10] The moderate emission intensity decrease of **2** and **3** with fluoride ions may be attributed partially to the dynamic association and dissociation process of the fluoride ions with the boron atom that increases the rate of nonradiative decay through thermal vibrational pathways. In addition, a new fluorescent band appears at λ_{max} = ∼370 nm with the addition of fluoride. TD-DFT calculation results for the fluoride adducts of $[NH_4][\mathbf{2F}]$ and $[NH_4][\mathbf{3F}]$ at the ground state indicate that the frontier orbitals are similar to those of **2** and **3**, but the Pt d orbital contributions are significantly decreased approximately 10−12%, which may also account for the decreased phosphorescent efficiency. In addition, the computational data confirmed that the T_1 state of the fluoride adducts has similar orbital contributions as that of **2** and **3**, although the energy is red-shifted by ∼0.2 eV, providing a plausible explanation for why the phosphorescent spectra **2** and **3** experience little change on the addition of fluoride. On the basis of the computational data, the new fluorescence band at 370 nm in the fluoride adducts may be assigned to the S_{10} transition. Complete calculation results for the fluoride adducts are provided in the Supporting Information.

The fluoride adducts $\mathbf{2F}^-$ and $\mathbf{3F}^-$ were observed and confirmed by ^{1}H and ^{19}F NMR spectra (see Supporting Information). In the ^{19}F NMR spectra, one characteristic

dx.doi.org/10.1021/om301112u | *Organometallics* XXXX, XXX, XXX−XXX

chemical shift at −174.7 ppm for $2F^-$ and −174.5 ppm for $2F^-$ was observed, which is similar to the previously reported chemical shifts of fluoride adducts with a $BMes_2$ group (typically in the range −175 to −180 ppm).[6b,c,10] No typical Pt−F signals[24] were observed in the ^{19}F NMR spectra, which further supports that the fluoride anion is bound to the boron center in the Pt(II) compounds. The results of the fluoride titration experiments further support that the lowest triplet states of compounds **2** and **3** do not involve the $BMes_2$ group.

CONCLUSIONS

We have shown that the replacement of an acac ancillary ligand by a picolinate ligand has a dramatic impact on the phosphorescent properties of the *m-Bppy*-based Pt(II) compounds, leading to a red shift of the emission energy and a substantial reduction of the emission quantum efficiency. A TD-DFT computational study and electrochemical and fluoride titration experiments consistently show that the low-lying LUMO level introduced by the picolinate ligand is the primary cause of this phenomenon, which results in no or little contributions from the $BMes_2$ group to the emissive states. The phosphorescence of the (*m-Bppy*)Pt(picolinate) compounds is mainly from charge transfer transitions from the phenyl ring of the ppy to the picolinate. In addition, the picolinate Pt(II) compounds display a greater tendency of intermolecular π-stacking, compared to the acac Pt(II) analogues. Thus, the picolinate ligand is not a suitable ancillary ligand in order to achieve efficient blue phosphorescent Pt(II) compounds based on $BMes_2$-functionalized ppy and the related chelate ligand. However, it may be used in achieving efficient orange or red phosphorescent BMes-N^C-chelate Pt(II) systems where the N^C-chelate ligand has a low-lying π^* level that is below that of the picolinate. The introduction of an R group on the pyridyl ring of the picolinate ligand is an effective strategy to minimize intermolecular stacking interactions of the Pt(II) compounds.

EXPERIMENTAL SECTION

General Information. All reactions were carried out under a dry nitrogen atmosphere using standard Schlenk techniques. All starting materials were purchased from either Aldrich Chemical Co. or Strem Chemicals, Inc. and used without further purification. ^1H and ^{13}C NMR spectra were recorded on a Bruker Avance 400 MHz spectrometer. UV−vis spectra were obtained on a Varian Cary 50 UV−visible spectrophotometer with all sample concentrations in the range of 10 μM. Excitation and emission spectra were recorded on a Photon Technologies International QuantaMaster model 2 spectrometer. Photoluminescent lifetimes were measured on a Photon Technology International Phosphorescent lifetime spectrometer, Timemaster C-631F equipped with a xenon flash lamp, and digital emission photon multiplier tube for both excitation and emission. All solutions for photophysical experiments were degassed under a nitrogen atmosphere. Solution quantum yields were calculated using optically dilute solutions ($A \approx 0.1$), using 9,10-diphenylanthracene ($\Phi = 0.950$)[18] as the standard for *m-Bppy* and *fac*-Ir(ppy)$_3$[19] for the platinum complexes in degassed CH_2Cl_2 at 298 K. Cyclic voltammetry was performed using a BAS CV-50W voltammetric analyzer with scan rates of either 50 or 100 mV/s. The electrolytic cell used was a conventional three-compartment cell, with a Pt working electrode, Pt wire auxiliary electrode, and Ag/AgCl reference electrode. The CV measurements were performed at room temperature using 0.10 M NBu_4PF_6 in DMF as the supporting electrolyte. The ferrocenium/ferrocene couple ($E^o = 0.55$ V) was used as the internal standard. The starting materials (3-bromophenyl)dimesitylborane,[8a] *m-Bppy*,[8a] bis-[dimethyl(μ-dimethylsulfide)platinum(II)],[25] and (*m-Bppy*)Pt(acac) (**1**)[11] were synthesized according to literature procedures.

The computational calculations were performed using the Gaussian09, revision B.01,[26] software package and the High Performance Computing Virtual Laboratory (HPCVL) at Queen's University. The ground-state geometries were fully optimized at the B3LYP[27] level using the LANL2DZ basis set for platinum metal and the 6-31G(d) basis set for all other atoms.[28] The initial geometric parameters in the calculations were employed from crystal structure data for geometry optimization. TD-DFT calculations were performed to obtain the vertical singlet and triplet excitation energies.

Synthesis of Pt(II) Complexes. The starting material $[PtMe_2(SMe_2)]_2$ (100 mg, 0.174 mmol) and the *m-Bppy* ligand (140 mg, 0.348 mmol) were dissolved in THF (15 mL), and this mixture was stirred for 2 h at room temperature. 2-Picolinic acid (64 mg, 0.522 mmol) [or 4-methyl-2-picolinic acid] dissolved in THF (10 mL) solution was added to this mixture. The reaction mixture was further stirred for 48 h at the same condition. After removal of the solvent, the resulting mixture was extracted with dichloromethane, washed with water, dried over magnesium sulfate, and filtered. The filtrate was concentrated under reduced pressure and purified by column chromatography on silica gel, eluting with ethyl acetate, obtaining the Pt(II) compounds in 70−72% yields as pale yellow solids.

*(m-Bppy)Pt(pic) (**2**).* Compound **2** was obtained in 72% yield as a yellow solid (180 mg, 0.250 mmol) from 2-picolic acid. ^1H NMR (400 MHz, $CDCl_3$, 25 °C, TMS): δ 9.14 (d, ^3J = 5.6 Hz, 1H), 9.10 (d, ^3J = 6.0 Hz, 1H), 8.13 (td, ^3J = 6.8 Hz, ^4J = 0.8 Hz, 1H), 8.07 (td, ^3J = 7.2 Hz, ^4J = 0.8 Hz, 1H), 7.73 (td, ^3J = 7.6 Hz, ^4J = 0.8 Hz, 1H), 7.56−7.53 (m, 2H), 7.50 (d, ^3J = 8.0 Hz, 1H), 7.43 (d, ^3J = 8.0 Hz, 1H), 7.28 (d, ^3J = 8.0 Hz, 1H), 7.08 (td, ^3J = 6.8 Hz, ^4J = 0.8 Hz, 1H), 6.77 (s, 4H), 2.25 (s, 6H), 1.98 (s, 12H). ^{13}C NMR (100 MHz, $CDCl_3$, 25 °C, TMS): δ 171.9, 166.5, 154.3, 150.0, 148.8, 146.3, 144.2, 141.6, 141.2, 140.8, 139.4, 138.5, 138.4, 131.8, 131.7, 128.2, 127.7, 122.0, 118.8, 23.6, 21.3. Anal. Calcd (%) for $C_{35}H_{33}BN_2O_2Pt$: C 58.42, H 4.62, N 3.89. Found: C 58.18, H, 4.71, N 3.72.

*(m-Bppy)Pt(Me-pic) (**3**).* Complex **3** was prepared in 70% yield as a yellow solid (179 mg, 0.243 mmol) from 4-methyl-2-picolinic acid. ^1H NMR (400 MHz, $CDCl_3$, 25 °C, TMS): δ 9.12 (d, ^3J = 5.6 Hz, 1H), 8.96 (d, ^3J = 5.6 Hz, 1H), 7.97 (d, ^4J = 1.2 Hz, 1H), 7.74 (td, ^3J = 7.6 Hz, ^4J = 1.2 Hz, 1H), 7.58 (s, 1H), 7.50 (d, ^3J = 8.0 Hz, 1H), 7.44 (d, ^3J = 8.0 Hz, 1H), 7.34 (dd, ^3J = 5.6 Hz, ^4J = 1.6 Hz, 1H), 7.28 (dd, ^3J = 7.6 Hz, ^4J = 1.2 Hz, 1H), 7.06 (td, ^3J = 6.0 Hz, ^4J = 0.8 Hz, 1H), 6.77 (s, 4H), 2.42 (s, 3H), 2.26 (s, 6H), 2.02 (s, 12H). ^{13}C NMR (100 MHz, $CDCl_3$, 25 °C, TMS): δ 178.2, 166.5, 153.6, 152.1, 149.9, 148.1, 146.3, 144.3, 141.6, 140.8, 139.3, 138.5, 138.4, 131.8, 129.1, 128.3, 128.2, 122.0, 118.7, 23.6, 21.6, 21.3. Anal. Calcd (%) for $C_{36}H_{35}BN_2O_2Pt$: C 58.94, H 4.81, N 3.82. Found: C 58.60, H 4.85, N 3.65.

X-ray Crystallographic Analysis. Single crystals of **2** and **3** were mounted on glass fibers and were collected on a Bruker Apex II single-crystal X-ray diffractometer with graphite-monochromated Mo Kα radiation, operating at 50 kV and 30 mA and at 180 K. Data were processed on a PC with the aid of the Bruker SHELXTL software package (version 6.10)[29] and corrected for absorption effects. Compounds **2** and **3** belong to the monoclinic crystal space group $P2_1/c$ and the triclinic space group $P\bar{1}$, respectively. The crystal of **2** contains disordered hexane solvent molecules (0.5 hexane per molecule of **2**), which could not be modeled successfully. As a result, the contributions from the disordered solvent molecules were removed by the Platon Squeeze routine.[30] All non-hydrogen atoms were refined anisotropically. Complete crystal structure data can be found in the Supporting Information. The crystal data of **2** and **3** have been deposited at the Cambridge Crystallographic Data Center (CCDC 910735 and 910736).

ASSOCIATED CONTENT

Supporting Information

NMR spectra, electrochemical data, fluoride titration data, crystal structural data, and TD-DFT computational data. This

dx.doi.org/10.1021/om301112u | *Organometallics* XXXX, XXX, XXX−XXX

material is available free of charge via the Internet at http://pubs.acs.org.

AUTHOR INFORMATION

Corresponding Author

*E-mail: wangs@chem.queensu.ca.

Notes

The authors declare no competing financial interest.

ACKNOWLEDGMENTS

We thank the Natural Sciences and Engineering Research Council for financial support. S.W. thanks the Canada Council for the Arts for the Killam Research Fellowship.

REFERENCES

(1) (a) Lequan, M.; Lequan, R. M.; Ching, K. C. *J. Mater. Chem.* **1991**, *1*, 997−999. (b) Yuan, Z.; Taylor, N. J.; Ramachandran, R.; Marder, T. B. *Appl. Organomet. Chem.* **1996**, *10*, 305−316. (c) Entwistle, C. D.; Marder, T. B. *Angew. Chem., Int. Ed.* **2002**, *41*, 2927−2931. (d) Entwistle, C. D.; Marder, T. B. *Chem. Mater.* **2004**, *16*, 4574−4585. (e) Liu, Z. Q.; Fang, Q.; Cao, D. X.; Wang, D.; Xu, G. B. *Org. Lett.* **2004**, *6*, 2933−2936. (f) Stahl, R.; Lambert, C.; Kaiser, C.; Wortmann, R.; Jakober, R. *Chem.—Eur. J.* **2006**, *12*, 2358−2370. (g) Yuan, Z.; Entwistle, C. D.; Collings, J. C.; Albesa-Jové, D.; Batsanov, A. S.; Howard, J. A. K.; Kaiser, H. M.; Kaufmann, D. E.; Poon, S. Y.; Wong, W. Y.; Jardin, C.; Fathallah, S.; Boucekkine, A.; Halet, J. F.; Taylor, N. J.; Marder, T. B. *Chem.—Eur. J.* **2006**, *12*, 2758−2771. (h) Matsumi, N.; Chujo, Y. *Polym. J.* **2008**, *40*, 77−89. (i) Collings, J. C.; Poon, S. Y.; Droumaguet, C. L.; Charlot, M.; Katan, C.; Plåsson, L. O.; Beeby, A.; Msely, J. A.; Kaiser, H. M.; Kaufmann, D.; Wong, W. Y.; Blanchard-Desce, M.; Marder, T. B. *Chem.—Eur. J.* **2009**, *15*, 198−208.

(2) (a) Noda, T.; Shirota, Y. *J. Am. Chem. Soc.* **1998**, *120*, 9714−9715. (b) Noda, T.; Ogawa, H.; Shirota, Y. *Adv. Mater.* **1999**, *11*, 283−285. (c) Shirota, Y.; Kinoshita, M.; Noda, T.; Okumoto, K.; Ohara, T. *J. Am. Chem. Soc.* **2000**, *122*, 11021−11022. (d) Shirota, Y. *J. Mater. Chem.* **2005**, *15*, 75−93. (e) Wakamiya, A.; Mori, K.; Yamaguchi, S. *Angew. Chem., Int. Ed.* **2007**, *46*, 4273−4276.

(3) (a) Yamaguchi, S.; Shirasaka, T.; Akiyama, S.; Tamao, K. *J. Am. Chem. Soc.* **2002**, *124*, 8816−8817. (b) Solé, S.; Gabbaï, F. P. *Chem. Commun.* **2004**, 1284−1285. (c) Parab, K.; Venkatasubbaiah, K.; Jäkle, F. *J. Am. Chem. Soc.* **2006**, *128*, 12879−12885. (d) Chiu, C.-W.; Gabbaï, F. P. *J. Am. Chem. Soc.* **2006**, *128*, 14248−14249. (e) Hudnall, T. W.; Gabbaï, F. P. *J. Am. Chem. Soc.* **2007**, *129*, 11978−11986. (f) Hudnall, T. W.; Kim, Y.-M.; Bebbington, M. W. P.; Bourissou, D.; Gabbaï, F. P. *J. Am. Chem. Soc.* **2008**, *130*, 10890−10891. (g) Zhou, G.; Baumgarten, M.; Müllen, K. *J. Am. Chem. Soc.* **2008**, *130*, 12477−12484. (h) Wade, C. R.; Broomsgrove, A. E. J.; Aldridge, S.; Gabbaï, F. P. *Chem. Rev.* **2010**, *110*, 3958−3984.

(4) (a) Chiu, C. W.; Gabbaï, F. P. *J. Am. Chem. Soc.* **2006**, *128*, 14248−14249. (b) Jia, W. L.; Bai, D. R.; McCormick, T.; Liu, Q. D.; Motala, M.; Wang, R.; Seward, C.; Tao, Y.; Wang, S. *Chem.—Eur. J.* **2004**, *10*, 994−1006. (c) Jia, W. L.; Feng, X. D.; Bai, D. R.; Lu, Z. H.; Wang, S.; Vamvounis, G. *Chem. Mater.* **2005**, *17*, 164−170. (d) Jia, W. L.; Moran, M. J.; Yuan, Y.-Y.; Lu, Z. H.; Wang, S. *J. Mater. Chem.* **2005**, *15*, 3326−3333. (e) Li, F. H.; Jia, W. L.; Wang, S.; Zhao, Y. Q.; Lu, Z. H. *J. Appl. Phys.* **2008**, *103*, 034509/1−034509/6. (f) Elbing, M.; Bazan, G. C. *Angew. Chem., Int. Ed.* **2008**, *47*, 834−838.

(5) (a) Liu, X. Y.; Bai, D. R.; Wang, S. *Angew. Chem., Int. Ed.* **2006**, *45*, 5475−5478. (b) Bai, D.-R.; Liu, X.-Y.; Wang, S. *Chem.—Eur. J.* **2007**, *13*, 5713−5723.

(6) (a) Sakuda, E.; Funahashi, A.; Kitamura, N. *Inorg. Chem.* **2006**, *45*, 10670−10677. (b) Zhao, S.-B.; McCormick, T.; Wang, S. *Inorg. Chem.* **2007**, *46*, 10965−10967. (c) Sun, Y.; Ross, N.; Zhao, S. B.; Huszarik, K.; Jia, W. L.; Wang, R. Y.; Macartney, D.; Wang, S. *J. Am. Chem. Soc.* **2007**, *129*, 7510−7511. (d) Zhou, G. J.; Ho, C. L.; Wong, W. Y.; Wang, Q.; Ma, D. G.; Wang, L. X.; Lin, Z. Y.; Marder, T. B.; Beeby, A. *Adv. Funct. Mater.* **2008**, *18*, 499−511. (e) You, Y.; Park, S. Y. *Dalton Trans.* **2009**, 1267−1282. (f) Zhou, G. J.; Wang, Q.; Wang, X. Z.; Ho, C.-L.; Wong, W.-Y.; Ma, D. G.; Wang, L. X.; Lin, Z. Y. *J. Mater. Chem.* **2010**, *20*, 7472. (g) Hudson, Z. M.; Sun, C.; Helander, M. G.; Amarne, H.; Lu, Z.-H.; Wang, S. *Adv. Funct. Mater.* **2010**, *20*, 3426−3439. (h) Hudson, Z. M.; Helander, M. G.; Lu, Z.-H.; Wang, S. *Chem. Commun.* **2011**, *47*, 755−757. (i) Wang, Z. B; Helander, M. G.; Hudson, Z. M.; Wang, S.; Lu, Z. H. *Appl. Phys. Lett.* **2011**, *98*, 213301/1−213301/3. (j) Hudson, Z. M.; Wang, S. *Dalton Trans.* **2011**, *40*, 7805−7816.

(7) (a) Me laïmi, M.; Gabbaï, F. P. *J. Am. Chem. Soc.* **2005**, *127*, 9680−9681. (b) Lee, M. H.; Gabbaï, F. P. *Inorg. Chem.* **2007**, *46*, 8132−8138.

(8) (a) You, Y.; Park., S. Y. *Adv. Mater.* **2008**, *20*, 3820−3826. (b) Zhao, Q.; Li, F. Y.; Liu, S. J.; Yu, M. X.; Liu, Z. Q.; Yi, T.; Huang, C. H. *Inorg. Chem.* **2008**, *47*, 9256−9264. (c) Vadavi, R. S.; Kim, H.; Lee, K. M.; Kim, T.; Lee, J.; Lee, Y. S.; Lee, M. H. *Organometallics* **2012**, *31*, 31−34.

(9) (a) Lam, S. T.; Zhu, N.; Yam, V. W.-W. *Inorg. Chem.* **2009**, *48*, 9664−9670. (b) Ito, A.; Kang, Y. Y.; Saito, S.; Sakuda, E.; Kitamura, N. *Inorg. Chem.* **2012**, *51*, 7722−7732. (c) Wade, C. R.; Gabbaï, F. P. *Inorg. Chem.* **2010**, *49*, 714−720. (d) Sun, Y.; Hudson, Z. M.; Rao, Y. L.; Wang, S. *Inorg. Chem.* **2011**, *50*, 3373−3378.

(10) (a) Sun, Y.; Wang, S. *Inorg. Chem.* **2009**, *48*, 3755−3767. (b) Rao, Y. -L.; Wang, S. *Inorg. Chem.* **2009**, *48*, 7698−7713. (c) Sun, Y.; Wang, S. *Inorg. Chem.* **2010**, *49*, 4394−4404. (d) Hudson, Z. M.; Wang, S. *Organometallics* **2011**, *30*, 4695−4701.

(11) Rao, Y.-L.; Schoenmakers, D.; Chang, Y.-L.; Lu, J.-S.; Lu, Z.-H.; Kang, Y.; Wang, S. *Chem.—Eur. J.* **2012**, *18*, 11306−11316.

(12) (a) Wang, Y.; Deng, X.; Liu, Y.; Ni, M.; Liu, M.; Tan, H.; Li, X.; Zhu, W.; Cao, Y. *Tetrahedron* **2011**, *67*, 2118−2124. (b) Li, X.; Liu, Y.; Luo, J.; Zhang, Z.; Shi, D.; Chen, Q.; Wang, Y.; He, J.; Li, J.; Lei, G.; Zhu, W. *Dalton Trans.* **2012**, *41*, 2972−2978.

(13) (a) Gu, X.; Fei, T.; Zhang, H.; Xu, H.; Yang, B.; Ma, Y.; Liu, X. J. *Chem. Phys. A* **2008**, *112*, 8387−8393. (b) Rausch, A. F.; Thompson, M. E.; Yersin, H. *J. Phys. Chem. A* **2009**, *113*, 5927−5932.

(14) (a) Rausch, A. F.; Homeier, H. H. H.; Djurovich, P. I.; Thompson, M. E.; Yersin, H. *Proc. SPIEs-Int. Soc. Opt. Eng.* **2007**, *6655*, 66550F. (b) Rausch, A. F.; Thompson, M. E.; Yersin, H. *Inorg. Chem.* **2009**, *48*, 1928−1937.

(15) Wang, N.; Hudson, Z. M.; Wang, S. *Organometallics* **2010**, *29*, 4007−4011.

(16) Hudson, Z. M.; Blight, B. A.; Wang, S. *Org. Lett.* **2012**, *14*, 1700−1703.

(17) Chang, S.-Y.; Cheng, Y.-M.; Chi, Y.; Lin, Y.-C.; Jiang, C.-M.; Lee, G.-H.; Chou, P.-T. *Dalton Trans.* **2008**, 6901−6911.

(18) Demas, N. J.; Crosby, G. A. *J. Am. Chem. Soc.* **1970**, *92*, 7262−7270.

(19) Sajoto, T.; Djurovich, P. I.; Tamayo, A. B.; Oxgaard, J.; Goddard, W. A., III; Thompson, M. E. *J. Am. Chem. Soc.* **2009**, *131*, 9813−9822.

(20) (a) Shao, P.; Li, Y.; Azenkeng, A.; Hoffmann, M. R.; Sun, W. *Inorg. Chem.* **2009**, *48*, 2407−2419. (b) Wen, H. -M.; Wu, Y.-H.; Fan, Y.; Zhang, L.; Chen, C.-N.; Chen, Z.-N. *Inorg. Chem.* **2010**, *49*, 2210−2221. (c) Wang, X.; Goeb, S.; Ji, Z.; Castellano, F. N. *J. Phys. Chem. B* **2010**, *114*, 14440−14449.

(21) (a) D'Andrade, B.; Forrest, S. R. *Chem. Phys.* **2003**, *286*, 321−335. (b) Ma, B.; Djurovich, P. I.; Garon, S.; Alleyne, B.; Thompson, M. E. *Adv. Funct. Mater.* **2006**, *16*, 2438−2446. (c) Kim, D.; Brédas, J.-L. *J. Am. Chem. Soc.* **2009**, *131*, 11371−11380.

(22) Chen, C.-P.; Chan, S.-H.; Chao, T.-C.; Ting, C.; Ko, B.-T. *J. Am. Chem. Soc.* **2008**, *130*, 12828−12833.

(23) Connors, K. A. *Binding Constants: The Measurement of Molecular Complex Stability Constants*; John Wiley and Sons: *New York*, 1987; pp 147−160.

(24) (a) Clark, H. C. S.; Fawcett, J.; Holloway, J. H.; Hope, E. G.; Peck, L. A.; Russell, D. R. *J. Chem. Soc., Dalton Trans.* **1998**, 1249−1252. (b) Cross, R. J.; Haupt, M.; Rycroft, D. S.; Winfield, J. M. *J.*

Organomet. Chem. **1999**, *587*, 195−199. (c) Jasim, S. A.; Perutz, R. N. *J. Am. Chem. Soc.* **2000**, *122*, 8685−8693.
(25) Hill, G. S.; Irwin, M. J.; Levy, C. J.; Rendina, L. M.; Puddephatt, R. J. *Inorg. Synth.* **1998**, *32*, 148−153.
(26) Frisch, M. J.; Trucks, G. W.; Schlegel, H. B.; Scuseria, G. E.; Robb, M. A.; Cheeseman, J. R.; Scalmani, G.; Barone, V.; Mennucci, B.; Petersson, G. A.; Nakatsuji, H.; Caricato, M.; Li, X.; Hratchian, H. P.; Izmaylov, A. F.; Bloino, J.; Zheng, G.; Sonnenberg, J. L.; Hada, M.; Ehara, M.; Toyota, K.; Fukuda, R.; Hasegawa, J.; Ishida, M.; Nakajima, T.; Honda, Y.; Kitao, O.; Nakai, H.; Vreven, T.; Montgomery, J. A., Jr.; Peralta, J. E.; Ogliaro, F.; Bearpark, M.; Heyd, J. J.; Brothers, E.; Kudin, K. N.; Staroverov, V. N.; Keith, T.; Kobayashi, R.; Normand, J.; Raghavachari, K.; Rendell, A.; Burant, J. C.; Iyengar, S. S.; Tomasi, J.; Cossi, M.; N. Rega, N.; Millam, J. M.; Klene, M.; Knox, J. E.; Cross, J. B.; Bakken, V.; Adamo, C.; Jaramillo, J.; Gomperts, R.; Stratmann, R. E.; Yazyev, O.; Austin, A. J.; Cammi, R.; Pomelli, C.; Ochterski, J. W.; Martin, R. L.; Morokuma, K.; Zakrzewski, V. G.; Voth, G. A.; Salvador, P.; Dannenberg, J. J.; Dapprich, S.; Daniels, A. D.; Farkas, O.; Foresman, J. B.; Ortiz, J. V.; Cioslowski, J.; Fox, D. J. *Gaussian09*, revision B.01; Gaussian, Inc.: Wallingford, CT, 2010.
(27) (a) Lee, C.; Yang, W.; Parr, R. G. *Phys. Rev. B* **1988**, *37*, 785−789. (b) Becke, A. D. *J. Chem. Phys.* **1993**, *98*, 5648−5652.
(28) Hay, P. J. *J. Phys. Chem. A* **2002**, *106*, 1634−1641.
(29) *SHELXTL* Version 6.14; Bruker AXS: Madison, WI, 2000−2003.
(30) (a) Sluis, P. D. V.; Spek, A. L. *Acta Crystallogr.* **1990**, *A46*, 194−201. (b) Spek, A. L. *J. Appl. Crystallogr.* **2003**, *36*, 7−13. (c) Spek, A. L. *PLATON a Multipurpose Crystallographic Tool*; Utrecht University: Utrecht, The Netherlands, 2006.